

# Reflection of neuroblastoma intratumor heterogeneity in the new OHC-NB1 disease model

Theresa M. Thole<sup>1</sup>, Joern Toedling<sup>1</sup>, Annika Sprüssel<sup>1</sup>, Sebastian Pfeil<sup>1</sup>, Larissa Savelyeva<sup>2</sup>, David Capper<sup>3</sup>, Clemens Messerschmidt<sup>4</sup>, Dieter Beule<sup>4</sup>, Stefanie Groeneveld-Krentz<sup>1</sup>, Cornelia Eckert<sup>1</sup>, Guido Gamba<sup>5,6,7,8</sup>, Anton G. Henssen<sup>1,9</sup>, Sabine Finkler<sup>1</sup>, Johannes H. Schulte<sup>1,7,8,9</sup>, Anja Sieber<sup>10,11</sup>, Nils Bluethgen<sup>9,10,11</sup>, Christian R. A. Regembrecht<sup>5,12</sup>, Annette Künkele<sup>1,9</sup>, Marco Lodrini<sup>1</sup>, Angelika Eggert<sup>1,7,8,9</sup> and Hedwig E. Deubzer<sup>1,7,8,9,13</sup>

<sup>1</sup>Department of Pediatric Hematology and Oncology, Charité - Universitätsmedizin Berlin, Berlin, Germany

<sup>2</sup>Research Group Neuroblastoma Genomics, German Cancer Research Center (DKFZ), Heidelberg, Germany

<sup>3</sup>Department of Neuropathology, Charité – Universitätsmedizin Berlin, Berlin, Germany

<sup>4</sup>Core Unit Bioinformatics, Berliner Institut für Gesundheitsforschung (BIH), Berlin, Germany

<sup>5</sup>CELLPhenomics GmbH, Berlin, Germany

<sup>6</sup>Charité Comprehensive Cancer Center (CCCC), Charité - Universitätsmedizin Berlin, Berlin, Germany

<sup>7</sup>German Cancer Consortium (DKTK), Berlin, Germany

<sup>8</sup>German Cancer Research Center (DKFZ), Heidelberg, Germany

<sup>9</sup>Berliner Institut für Gesundheitsforschung (BIH), Berlin, Germany

<sup>10</sup>Computational Modelling in Medicine, Charité – Universitätsmedizin Berlin, Institute for Pathology, Berlin, Germany

<sup>11</sup>IRI Life Sciences, Humboldt University Berlin, Berlin, Germany

<sup>12</sup>Department for Pathology, Medical Faculty, Otto-von-Guericke University of Magdeburg, Magdeburg, Germany

<sup>13</sup>Neuroblastoma Research Group, Experimental and Clinical Research Center (ECRC) of the Charité and the Max-Delbrück-Center for Molecular Medicine (MDC) in the Helmholtz Association, Berlin, Germany

Accurate modeling of intratumor heterogeneity presents a bottleneck against drug testing. Flexibility in a preclinical platform is also desirable to support assessment of different endpoints. We established the model system, OHC-NB1, from a bone marrow metastasis from a patient diagnosed with *MYCN*-amplified neuroblastoma and performed whole-exome sequencing on the source metastasis and the different models and passages during model development (monolayer cell line, 3D spheroid culture and subcutaneous xenograft tumors propagated in mice). OHC-NB1 harbors a *MYCN* amplification in double minutes, 1p deletion, 17q gain and diploid karyotype, which persisted in all models. A total of 80–540 single-nucleotide variants (SNVs) was detected in each sample, and comparisons between the source metastasis and models identified 34 of 80 somatic SNVs to be propagated in the models. Clonal reconstruction using the combined copy number and SNV data revealed marked clonal heterogeneity in the originating metastasis, with four clones being reflected in the model systems. The set of OHC-NB1 models represents 43% of somatic SNVs and 23% of the cellularity in the originating metastasis with varying clonal compositions, indicating that heterogeneity is partially preserved in our model system.

T.M.T. and J.T. contributed equally to this work

Additional Supporting Information may be found in the online version of this article.

**Key words:** embryonal tumor, single-nucleotide variant analysis, copy number variation analysis, clonal reconstruction, *MYCN* amplification, preclinical drug testing

**Abbreviations:** CNV: copy-number variation; FISH: fluorescence *in situ* hybridization; INRG: International Neuroblastoma Risk Group; SNV: single-nucleotide variant; WES: whole-exome sequencing

**Conflict of interest:** None.

**Grant sponsor:** Berlin Institute of Health; **Grant number:** CRG TERMINATE-NB; **Grant sponsor:** German Federal Ministry of Education and Research (BMBF); **Grant numbers:** ERA-Net ERACoSysMED project OPTIMIZE-NB, 031L0087B, e:MED SYSMED-NB, 01ZX1607E, 01ZX1607A, ZiSSTrans, 02NUK047E

This is an open access article under the terms of the Creative Commons Attribution-NonCommercial-NoDerivs License, which permits use and distribution in any medium, provided the original work is properly cited, the use is non-commercial and no modifications or adaptations are made.

DOI: 10.1002/ijc.32572

**History:** Received 26 Mar 2019; Accepted 5 Jul 2019; Online 15 Jul 2019

**Correspondence to:** Hedwig E. Deubzer, Charité – Universitätsmedizin Berlin, Department of Pediatric Hematology and Oncology, Augustenburger Platz 1, 13353 Berlin, Germany, Tel.: ++49-30-450-616-157, E-mail: hedwig.deubzer@charite.de

**What's new?**

Intratumor heterogeneity is becoming an accepted feature of high-risk tumors but models reliably capturing this feature remain elusive. Here the authors developed *in vitro* and *in vivo* neuroblastoma models from a single aspirate of a neuroblastoma bone marrow metastasis and analyzed the germline patient background, the metastasis and the models via whole-exome sequencing. The new OHC-NB1 model system partly reflects the genetic and clonal heterogeneity of the initial biopsy and presents an important first step towards accurate preclinical modeling of neuroblastoma.

**Introduction**

Neuroblastoma, the most common extracranial solid tumor of childhood, still accounts for 12% of cancer-related deaths in the population under 15 years of age,<sup>1</sup> mostly due to therapy-resistant relapses of high-risk disease. These patients urgently need novel targeted therapies and therapy combinations, whose development requires extensive preclinical testing. *MYCN* oncogene amplification is the most frequent genetic aberration in high-risk neuroblastoma (40–50%),<sup>2</sup> typically accompanied by 1p36 deletion<sup>3</sup> and 17q gain.<sup>4</sup> Further genetically defined subgroups of high-risk neuroblastoma, each comprising 20–30% of tumors, are characterized by activating *TERT* rearrangements or *ATRX* mutations causing alternative lengthening of telomeres.<sup>5,6</sup> The gene encoding the ALK receptor tyrosine kinase is the most frequently mutated in neuroblastoma, with 9% of tumors bearing activating mutations.<sup>7</sup> Activating mutations in the RAS-MAPK pathway and genes involved in epithelial-mesenchymal transition frequently arise at relapse.<sup>8,9</sup> These differing molecular components of high-risk disease must be represented in models to support effective preclinical testing.

Deep sequencing on sequential solid and liquid biopsies revealed spatial and temporal genetic heterogeneity of copy-number variations (CNVs)<sup>10–12</sup> and *ALK* mutations<sup>13,14</sup> within individual patients. These recent findings underline the complexity of neuroblastoma genetics and pathogenesis, and have impact for disease monitoring and targeted therapy selection. The majority of models currently used in neuroblastoma research are monoclonal monolayer cultures established decades ago. Disease models reflecting intratumor heterogeneity would be ideal to test therapeutic efficacy. Our aim was to develop a set of neuroblastoma models derived from the same biosample to provide flexible support for different preclinical experimental designs and that is strongly representative of the heterogeneous clonal composition of the originating tissue.

**Materials and Methods****Patient diagnosis and sample origin**

A male patient, older than 18 months, had been diagnosed with *MYCN*-amplified INRG stage M neuroblastoma and was treated within the German Pediatric Oncology Group NB 2004 trial. The primary tumor site was thoracoabdominal with metastases detected in the bone marrow, liver and brain. The OHC-NB1 primary culture was derived from the first diagnostic bone marrow aspirate, which had 80% tumor cell infiltration. Parental

consent for the use of surplus biomaterial samples for research purposes is documented within the German Pediatric Oncology Group NB 2004 trial data.

**OHC-NB1 propagation in mice**

Cells suspended in 200  $\mu$ l Matrigel™ (BD Biosciences, Franklin Lakes, New Jersey, USA) were subcutaneously implanted into the flanks of 6-week-old female CB17-SCID mice for passages 1 and 2 and into NMRI-*Foxn1*<sup>tmu</sup> mice for passages 3–5. Tumor size was measured with a caliper. Tumor volume was calculated by  $\pi/6 (w1 \times w2 \times w2)$ , where *w1* was the largest tumor diameter and *w2* was the smallest tumor diameter. At each passage, xenograft tumors ( $n \geq 3$  per passage) were explanted, then split for four uses: (i) formalin fixation and paraffin embedding for histology and immunohistochemistry (details in Supplementary Materials and Methods), (ii) DNA isolation, (iii) fresh-frozen tissue storage in liquid nitrogen and (iv) preparation of one tumor for xenograft passaging (details in Supplementary Materials and Methods). Experiments conformed to all local, national and European regulatory standards and were approved by the local ethics committee.

**Cell culture**

Neuroblastoma cells in the bone marrow sample were enriched *via* density centrifugation through Ficoll (Biochrom, Berlin, Germany) and cultivated in DMEM (Lonza, Basel, Switzerland), supplemented with 10% fetal calf serum, 1% nonessential amino acids, 20 ng/ml recombinant EGF (PromoCell, Heidelberg, Germany) and 20 ng/ml recombinant FGF2 (PromoCell). Cells were frozen and stored in liquid nitrogen in 10% dimethyl sulfoxide in cell culture medium. To date, monolayer OHC-NB1 cells have been kept in culture for up to 18 months, corresponding to over 75 passages. BE(2)-C (RRID: CVCL\_V006), CLB-GA (RRID: CVCL\_9529), GI-ME-N (RRID: CVCL\_1232), IMR-32 (RRID: CV CL\_0346), IMR-5/75 (RRID: CVCL\_M473), Kelly (RRID: CVCL\_2092), LAN-6 (RRID: CV CL\_1363), SH-EP (RRID: CVCL\_0524), SH-SY5Y (RRID: CVCL\_0019) and SK-N-FI cells (RRID: CVCL\_1702) were cultivated as described.<sup>5,15</sup> The IMR5/75 cell line is a subclone of the IMR-32 cell line. The BE(2)-C cell line was purchased from the European Collection of Authenticated Cell Cultures (ECACC, Salisbury, UK). The GI-ME-N, IMR-32, Kelly, LAN-6 and SH-SY5Y cell lines were purchased from the German Collection of Microorganisms and Cell Cultures (DSMZ, Braunschweig, Germany). The SH-EP cell line was

kindly provided by the laboratory of M. Schwab (Neuroblastoma Genomics, German Cancer Research Center [DKFZ], Heidelberg, Germany), and the CLB-GA, IMR5/75 and SK-N-FI cell lines were kindly provided by M. Fischer (Children's Hospital of the University of Cologne, Cologne, Germany). All cell lines have been authenticated using STR or SNP profiling. Protocols for 3D spheroid propagation, qRT-PCR-based and fluorescence-activated cell sorting-based marker detection and routine contamination testing are supplied in the Supplementary Materials and Methods.

### Genomic analyses of OHC-NB1 models

The genomic composition of OHC-NB1 models was characterized using fluorescence *in situ* hybridization (FISH, details in Supplementary Materials and Methods) and whole-exome sequencing (WES). Libraries were prepared for WES using the Agilent SureSelect Human All Exon v6 kit (cat. No. 5190-8863) according to the manufacturer's instructions and sequenced in parallel in one HiSeq 4000 lane with 100 nt paired-end reads and 50x average coverage at the Genomics and Proteomics Core Facility of the German Cancer Research Center (Heidelberg, Germany). Read sequences and base quality scores were de-multiplexed and stored in Fastq format using Illumina bcl2fastq software.<sup>16</sup> *BWA-mem*<sup>17</sup> was used to map the reads from each sample against the human genome reference in assembly GRh37. Somatic single-nucleotide variants (SNVs) in each model system (original bone marrow metastasis, primary OHC-NB1 culture, xenograft passage 1 cells, OHC-NB1 monolayer culture, xenograft passage 4 cells, conditioned medium from xenograft passage 4 cells) were called with *Mutect*<sup>18</sup> using the germline sample (lymphocytes) as a control. Variants were annotated using *Jannovar*<sup>19</sup> and filtered for artifacts from PCR or sequencing using the *DKFZBiasFilter*.<sup>20</sup> To compile all available data for the complete set (union) of variants across all samples, the total numbers of reads supporting both the reference and variant alleles were computed from each BAM file using a combination of *samtools mpileup* and *bcftools call*. A smaller list of variants predicted to affect well-known cancer genes was generated by selecting mutations categorized as missense or nonsense variants in genes belonging to the cancer gene census list downloaded from the COSMIC database in January 2018, release v83.<sup>21</sup> Complete variant files in VCF format were imported into the R statistics software, and numbers of variants shared among samples were computed. CNVs were analyzed in paired fashion using the *CopywriteR* R package<sup>22</sup> and annotated using the CIViC database.<sup>23</sup> Regions gained or lost that had an absolute log<sub>2</sub> fold-change greater than 0.3 (compared to the germline control) were converted into standard Bed format and visualized using CIRCOS.<sup>24</sup> SNVs and CNVs were used to assess both clonal composition and evolution using the *QuantumClone* R package.<sup>25</sup> SNVs with a variant allele frequency of at least 10% in at least one sample were selected for computations, resulting in a total of 336 variants across the six samples. R statistics software was employed for statistical tests and visualizations.<sup>26</sup>

### Data availability

Raw sequencing data have been uploaded to the European Genome-phenome Archive (accession: EGAS00001003031).

## Results

### OHC-NB1 serves as an *in vitro* and *in vivo* experimental model

Here, we describe an adherent monolayer cell line, a 3D spheroid culture and a subcutaneous xenograft mouse model derived from the same infiltrated bone marrow aspirate from a patient diagnosed with INRG stage M neuroblastoma (Fig. 1). Monolayer OHC-NB1 cells exhibited a neuroblastic phenotype and proliferated with a doubling time of 42 hr when cultivated in medium supplemented with 10% fetal calf serum, epidermal growth factor and fibroblast growth factor 2 (Figs. 2a and 2b). In contrast, monolayer OHC-NB1 cells did not or hardly proliferate when cultured in medium supplemented with B27 serum-free supplement as a protein source or omitting the growth factors (Fig. 2c). If cultivated in Matrigel™, primary OHC-NB1 cells grew as nonadherent 3D spheroids (Fig. 2d). Primary OHC-NB1 cells were implanted into the flanks of CB17-SCID or NMRI-*Foxn1*<sup>tmu</sup> mice to create the xenograft model. Serial subcutaneous xenotransplantation through new host mice maintained tumorigenicity with a 100% take rate throughout five passages (Figs. 2e–2g). OHC-NB1 monolayers, 3D spheroids and xenografts show stable cultivation, and present a flexible system for preclinical experimental design.

### OHC-NB1 cells express protein markers characteristic of neuroblastoma

The expression of neuroblastoma marker proteins on the cell surface was assessed in fluorescence-activated cell sorting-based analyses of monolayer and 3D spheroid models as proof of tumor derivation. Neuroblastoma cells coexpress NCAM1 and GD2, a pattern that segregates neuroblastoma from other neuroectodermally derived pediatric tumors.<sup>27</sup> LICAM is a marker more widely expressed on many neuroectodermally derived tumors including neuroblastoma.<sup>28</sup> In monolayers, >95% of OHC-NB1 cells expressed NCAM1 and GD2 (Fig. 3a) and up to 85% expressed LICAM (Fig. 3a). NCAM1 and GD2 were coexpressed in >95% of OHC-NB1 monolayer cells (Fig. 3b). LICAM was coexpressed with either NCAM1 or GD2 in up to ~85% of OHC-NB1 monolayer cells (Fig. 3b). The percentage of cells dissociated from OHC-NB1 3D spheroids that coexpressed NCAM1 and GD2 was comparable to the monolayer model (Figs. 3c and 3d), but the fraction expressing LICAM was smaller (Figs. 3c and 3d). These data show that OHC-NB1 monolayer and spheroid models express characteristic markers for neuroblastoma.

NB84 and SYP, common markers in routine neuroblastoma diagnostics,<sup>29</sup> were immunohistochemically detected in OHC-NB1 xenograft tumors, demonstrating a representative neuroblastoma immunohistology (Fig. 4). The expression of druggable targets was investigated to identify signaling pathway alterations. High levels of activated (phosphorylated)

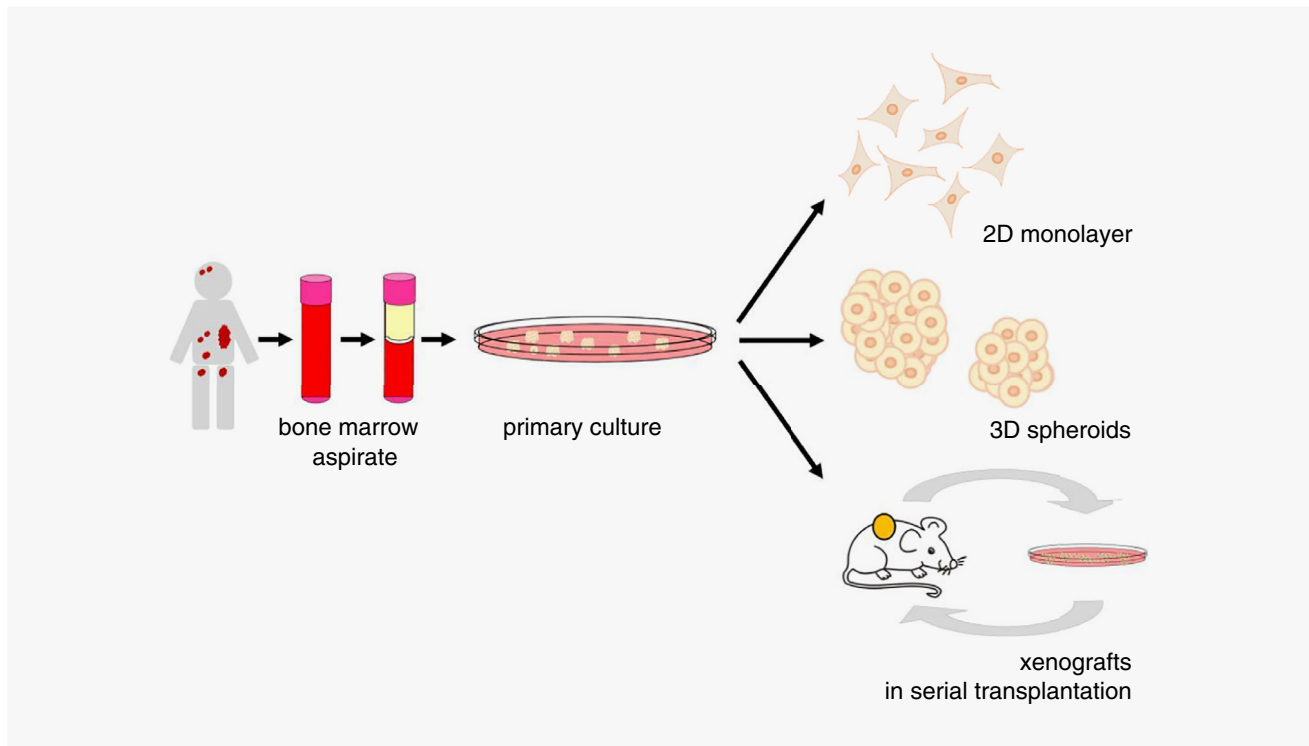


**Figure 1.** Schematic overview of OHC-NB1 models. The monolayer, spheroid and patient-derived xenograft models were all established from the same infiltrated bone marrow aspirate from a patient diagnosed with INRG stage M (metastasized) neuroblastoma.

EGFR were detected, with enhanced levels at the tumor margins (Fig. 4). In contrast, immunohistochemistry for phosphorylated AKT1 or RPS6KB1 indicated no evidence of PIK3CA/AKT1/MTOR pathway activation (Fig. 4). Actively cycling cells express MKI67,<sup>30</sup> which was detected in close to 100% of cells in OHC-NB1 xenografts (Fig. 4). As expected for cells harboring wild-type *TP53*, only 10–15% of cells in OHC-NB1 xenografts demonstrated transcriptionally active nuclearly localized *TP53* (Fig. 4). Expression of the CD9 cell surface glycoprotein, which was recently identified as a suppressor of the invasion-metastasis cycle in neuroblastoma,<sup>31</sup> was below the detection limit. OHC-NB1 xenograft tumors express characteristic neuroblastoma markers and biomarkers indicating overactive EGFR signaling.

#### **MYCN amplification is the leading genetic alteration in OHC-NB1 cells**

The OHC-NB1 genomic background was characterized using FISH and WES. Multicolor FISH illuminated a diploid male karyotype with gains at 2p and 17q and the three derivative chromosomes, der(1)t(1;2), der(20)t(1;20) and der(16)t(16;17) (Fig. 5a). FISH analysis with BAC probes specific for the *MYC* and *MYCN* loci revealed two *MYC* copies on chromosome 8q, two *MYCN* copies on chromosome 2p and *MYCN* amplification as double minutes (Fig. 5b), creating high *MYCN* levels that are comparable to those in established

*MYCN*-amplified neuroblastoma cell lines (Fig. S1a). *MYCN* amplification was associated with upregulated *TERT* expression as previously shown for other *MYCN*-amplified neuroblastoma cell lines and tumors (Fig. S1b).<sup>5,6</sup> *MYCN* amplifications and *TERT* rearrangements have been demonstrated to be mutually exclusive in high-risk neuroblastomas.<sup>5,6</sup> Targeted sequencing excluded genomic rearrangements proximal to *TERT* (data not shown), confirming the mutual exclusivity of *MYCN* amplifications and *TERT* rearrangements in our model. All genomic analyses pinpoint *MYCN* amplification as the leading genetic aberration in OHC-NB1.

#### **OHC-NB1 partially reflects the heterogeneity of the originating metastasis**

To understand how well each model reflects the source metastasis and track the dynamics of genetic heterogeneity in the model system, WES was performed on the source bone marrow metastasis and lymphocytes (as a germline control) from the patient as well as different OHC-NB1 culture models and passages during model development. The OHC-NB1 primary culture, xenograft passage 1, the monolayer model and the cellular fraction and medium conditioned by the intermittent *in vitro* culture of xenograft passage 4 were sequenced. CNV analysis identified a 1p deletion terminal to 1p22.3, 17q gain and *MYCN* amplification, all of which remained stable

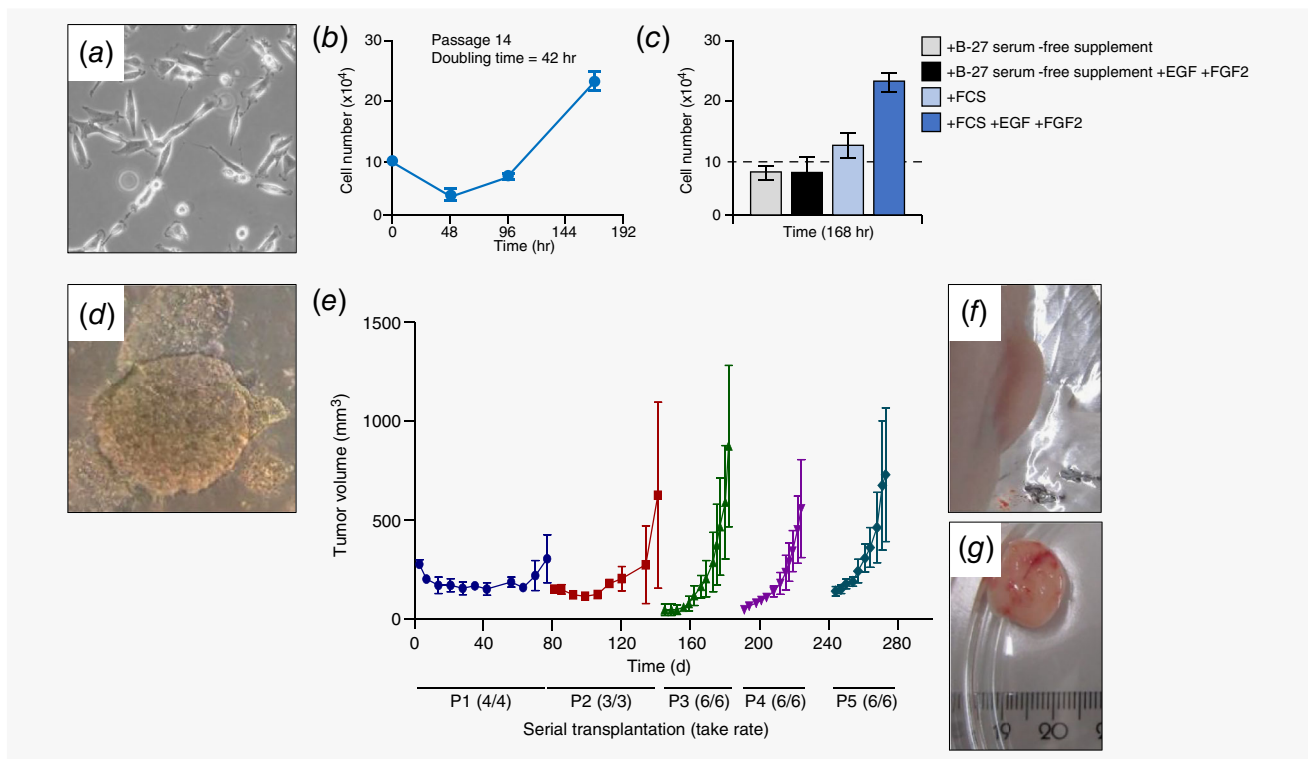


**Figure 2.** OHC-NB1 cells can be propagated *in vitro* and serially passaged as subcutaneous xenografts in mice. (a) Representative phase-contrast micrograph of OHC-NB1 monolayer model, passage 10. 200× magnification. (b) Growth curve for OHC-NB1 monolayer model in passage 14. (c) Comparison of OHC-NB1 monolayer cell numbers under different culture conditions. In total,  $10 \times 10^4$  cells were seeded (dotted line), and cell numbers were measured by semiautomated trypan blue staining 168 hr later. (d) Representative phase-contrast image of OHC-NB1 3D spheroid model. 10× magnification. (e) Growth curves for five serial passages (P) of OHC-NB1 cells as subcutaneous xenografts in CB17-SCID mice (P1 and P2) and NMRI-*Foxn1*<sup>nu</sup> mice (P3–P5). Engraftment of all tumors ( $n = 25$ ) in serial transplantation ( $n = 5$ ) is shown (mean  $\pm$  SEM). Subcutaneous xenograft tumor in a representative mouse are shown (f) before and (g) after preparation.

throughout all model systems (Fig. 5c). SNV analysis considered all SNVs, regardless of their potential effect on the protein coding sequence. A total of 80–540 (median: 153) SNVs were detected in each sample (Fig. 6a), of which the large majority were *bona fide* somatic SNVs since <5.4% of the identified SNVs were listed in databases compiled by large-scale sequencing efforts in healthy individuals (Table S2). Comparisons between the source metastasis and models identified 34 of 80 somatic SNVs to be propagated in the models (Fig. 6a), with 20 SNVs detected in all models and 14 detected in at least one model. The remaining 46 somatic SNVs present in the source metastasis were not represented in the models (Fig. 6a). SNVs specific to a model comprised 26% of SNVs in the primary culture and 46% in the monolayer model (Fig. 6a). Many specific SNVs were detected in xenograft passage 1 that were not propagated in later xenograft passages (Fig. 6a) and most likely represent one or more clones present only in xenograft passage 1 (Fig. 6c). We detected 34 SNVs in all models but not the source metastasis (Fig. 6b) that either arose in the primary culture or were below detection sensitivity in the source metastasis. Another eight SNVs identified in the source metastasis were detected in one or more models

but not the primary culture (Fig. 6b). This heterogeneity extended to nonsilent mutations in known cancer genes (Fig. S2). Deleterious mutations in *KAT6B*, *KDM6A* and *NOTCH2* are prominent but specific to the xenografts, while a mutation in *LSM14A* is present in the source bone marrow metastasis and xenograft samples, yet absent in other cultures (Fig. S2). Taken together, a *MYCN* amplification, 1p deletion, 17q gain and small SNV set were propagated from the originating metastasis through all OHC-NB1 models. Other SNVs harbored in the source metastasis were propagated in at least one model, indicating clonal heterogeneity is partially preserved in our model system.

To understand and compare the clonal composition of the source metastasis to those of the model systems, we assessed clonal composition in each sample and carried out clonal reconstruction using the combined CNV and SNV data. Marked clonal heterogeneity existed in the originating metastasis, with four clones (accounting for 23% of cellularity in the metastasis) being reflected in the model systems (Fig. 6c). The remaining 77% of cellularity in the source metastasis was lost after propagation. Clone #3, characterized by 72 SNVs, made up <10% of the originating metastasis,

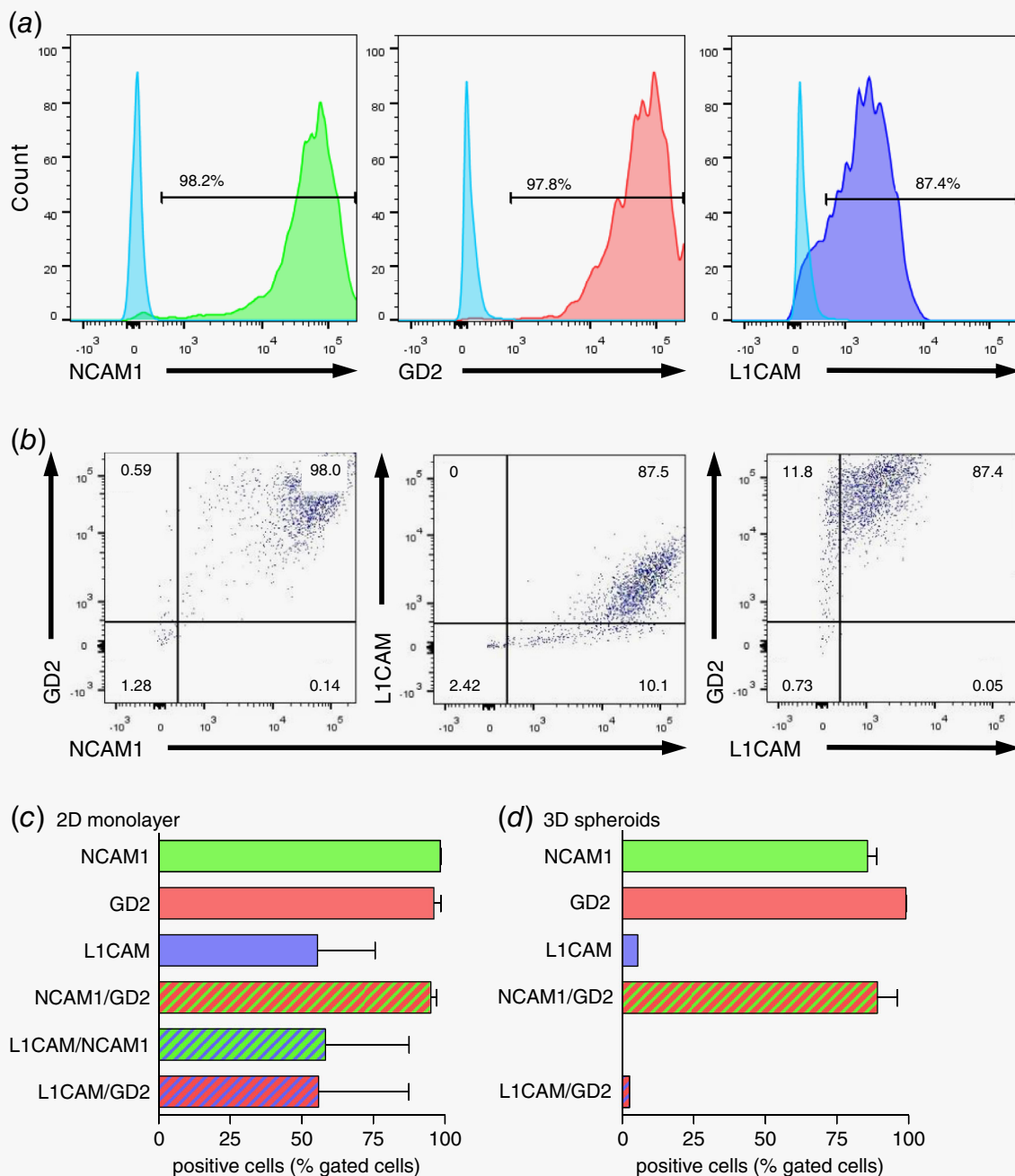


**Figure 3.** OHC-NB1 cells coexpress common neuroblastoma cell surface markers. (a) Fluorescence-activated cell sorting-based detection of NCAM1, GD2 and L1CAM expression in OHC-NB1 2D monolayer model shown as single-parameter histograms. (b) Representative dot plots of costained OHC-NB1 2D monolayer model cells. Neuroblastoma marker expression in the OHC-NB1 (c) 2D monolayer model and (d) 3D spheroid model. Fluorescence-activated cell sorting-based analysis of single markers (NCAM1, GD2, L1CAM) and costaining for two markers (NCAM1/GD2, L1CAM/NCAM1, L1CAM/GD2) is presented as the arithmetic mean  $\pm$  SD in bar graphs.

but underwent substantial clonal expansion before becoming the dominant clone in all models (Fig. 6c). Clone #5 was solely present in xenograft passage 1, and accounted for the large number of specific mutations in that sample (Figs. 6a and 6c). The other three clones present in the originating

metastasis made up elevated fractions of tumor cells in the xenograft and monolayer models (Fig. 6c). Taken together, the models represent 43% of somatic SNVs and 23% of the cellularity in the originating metastasis, with varying clonal compositions.

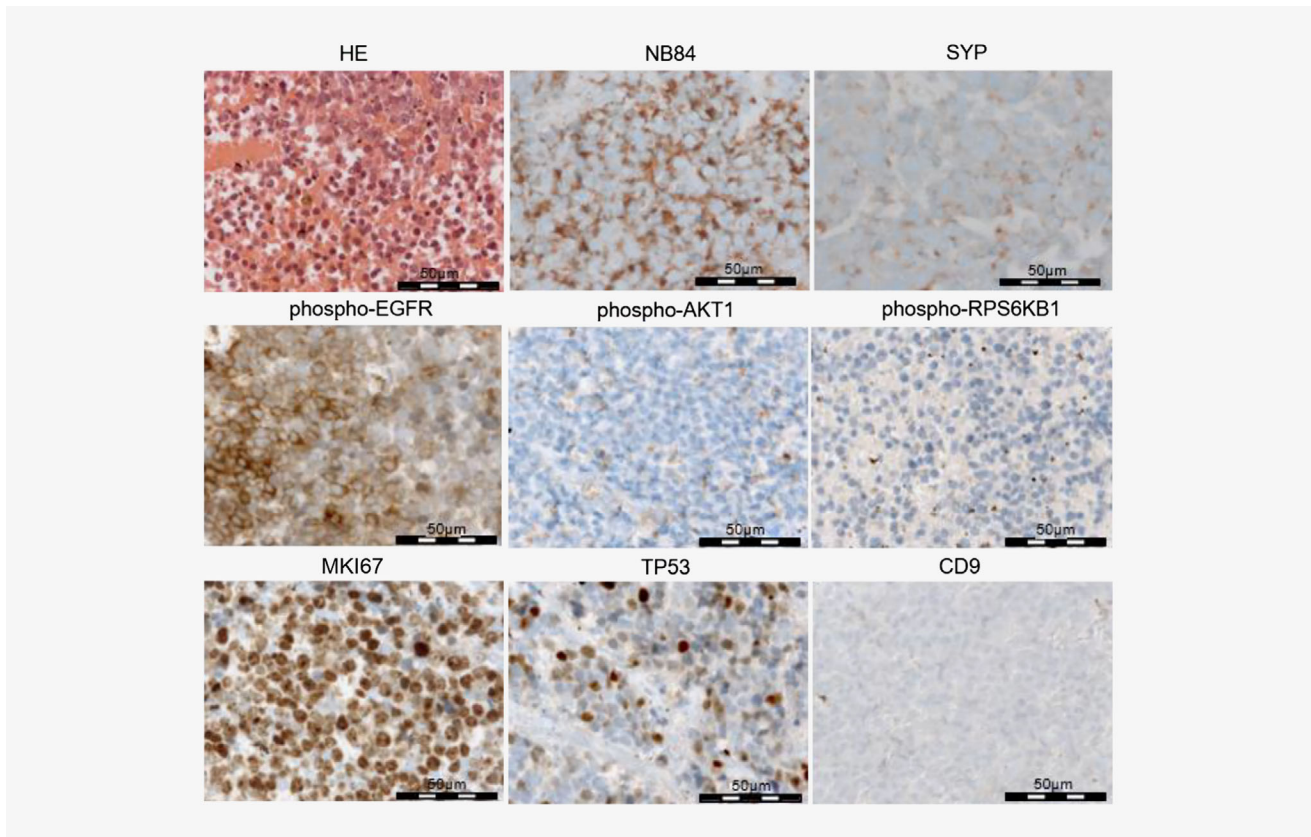


**Figure 4.** Expression of common neuroblastoma marker and druggable target proteins in OHC-NB1 xenografts. Representative micrographs are shown for OHC-NB1 xenograft model (passage 2) histology (HE: hematoxylin/eosin staining) and immunohistochemistry detecting the common neuroblastoma markers, NB84 (a 57 kD uncharacterized molecule used as a marker in routine pathology) and synaptophysin (SYP); the phosphorylated (activated) forms of the signaling proteins, epidermal growth factor receptor (EGFR), AKT serine/threonine kinase 1 (AKT1) and ribosomal protein S6 kinase B1 (RPS6KB1), in addition to the marker of proliferation Ki-67 (MKI67), subcellular localization of the tumor protein p53 (TP53) and expression of the transmembrane four superfamily member CD9 molecule (CD9). 630× magnification.

#### Targeted transcript expression analysis and phosphoproteomics reveal commonalities among the set of OHC-NB1 models

To investigate potential differences at the transcriptional level across the set of OHC-NB1 models and how they compare to established neuroblastoma cell lines, relative quantitative expression of *MYCN*, *LIN28B*, *TERT*, *BIRC5*, *HDAC5*, *NTRK2*, *DCX*, *GAP43*, *NEFL* and *NES* was assessed by qRT-PCR. The genes selected for targeted transcript expression analysis are oncogenic drivers in neuroblastoma (*MYCN*, *LIN28B*, *TERT*), *MYCN* targets (*BIRC5*, *HDAC5*) or play a role in neuroblastoma cell differentiation and stemness (*NTRK2*, *DCX*, *GAP43*, *NEFL*, *NES*). All 10 genes were similarly expressed in the primary culture, xenograft passages #1 and #4 as well as in the 3D spheroids and the 2D monolayer (Fig. S3). The overall expression pattern of OHC-NB1 most closely resembled the two *MYCN*-amplified neuroblastoma cell lines BE(2)-C and Kelly (Fig. S3). We performed a customized Luminex assay to compare protein phosphorylation in the PI3K/AKT and MEK/ERK signaling pathways among

the primary OHC-NB1 culture, 2D monolayer and 3D spheroids. Phosphorylation levels in the primary culture and 3D spheroids resembled each other more than those measured in the 2D monolayer, underlining the importance of exploiting the potential of 3D *in vitro* culture systems in future studies (Fig. S4). In summary, the mRNA and targeted phosphoproteome data presented here support the unbiased analysis of the set of OHC-NB1 models at the transcriptional and posttranslational level by OMICS technologies within the framework of a new study.

#### Discussion

Large-scale sequencing provided evidence of intratumor heterogeneity in the adherent OHC-NB1 monolayer model, a 3D spheroid model and serially transplantable xenograft tumor model in mice, which were all established from the same metastasis from an *MYCN*-amplified INRG stage M neuroblastoma (summarized as a model in Fig. S5). Capturing the landscape of spatial and intratumor heterogeneity in solid tumors has major implications for our understanding of

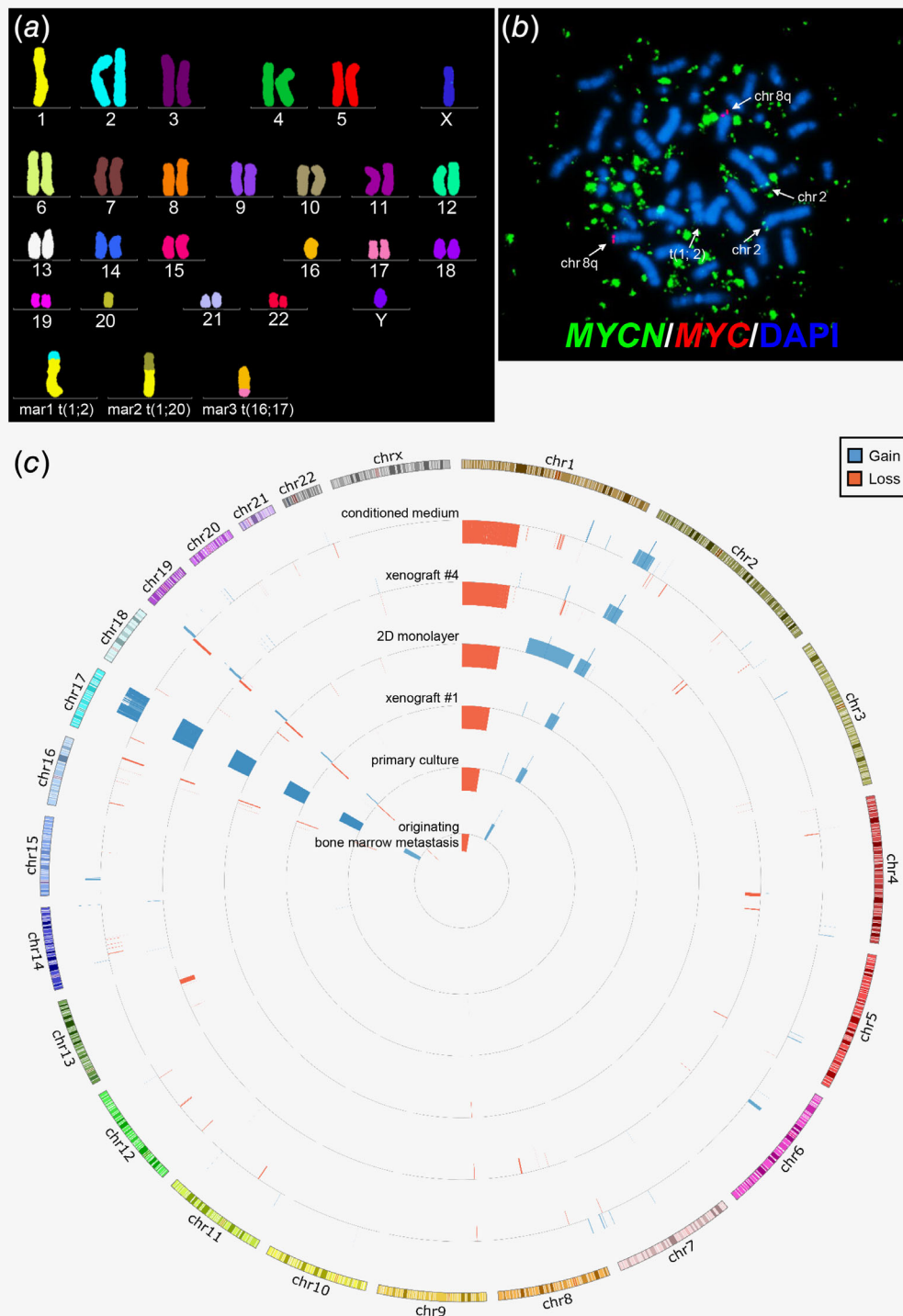


**Figure 5.** Genome-wide analysis of structural aberrations and CNVs in the OHC-NB1 model. (a) Representative multicolor FISH karyotype of the OHC-NB1 2D monolayer model employing three marker (mar) chromosomes, mar1 t(1;2), mar2 t(1;20) and mar3 t(16;17). (b) FISH-based detection of *MYCN* (green, BAC clone RP11-355H10) and *MYC* (red, BAC clone CTD-2034C18) in a chromosomal spread (stained with DAPI to detect DNA, blue) from the OHC-NB1 2D monolayer model, demonstrating extrachromosomal copies of the *MYCN* locus in the form of double minutes and a diploid complement of the *MYC* locus. (c) Circos plot reconstructed from whole-genome sequencing data and displaying CNVs in the originating bone marrow metastasis and different OHC-NB1 models or stages of OHC-NB1 model development. Xenograft #1, OHC-NB1 xenograft model passage 1; xenograft #4, OHC-NB1 xenograft model passage 4; conditioned medium, medium conditioned by the intermittent *in vitro* culture of xenograft passage 4.

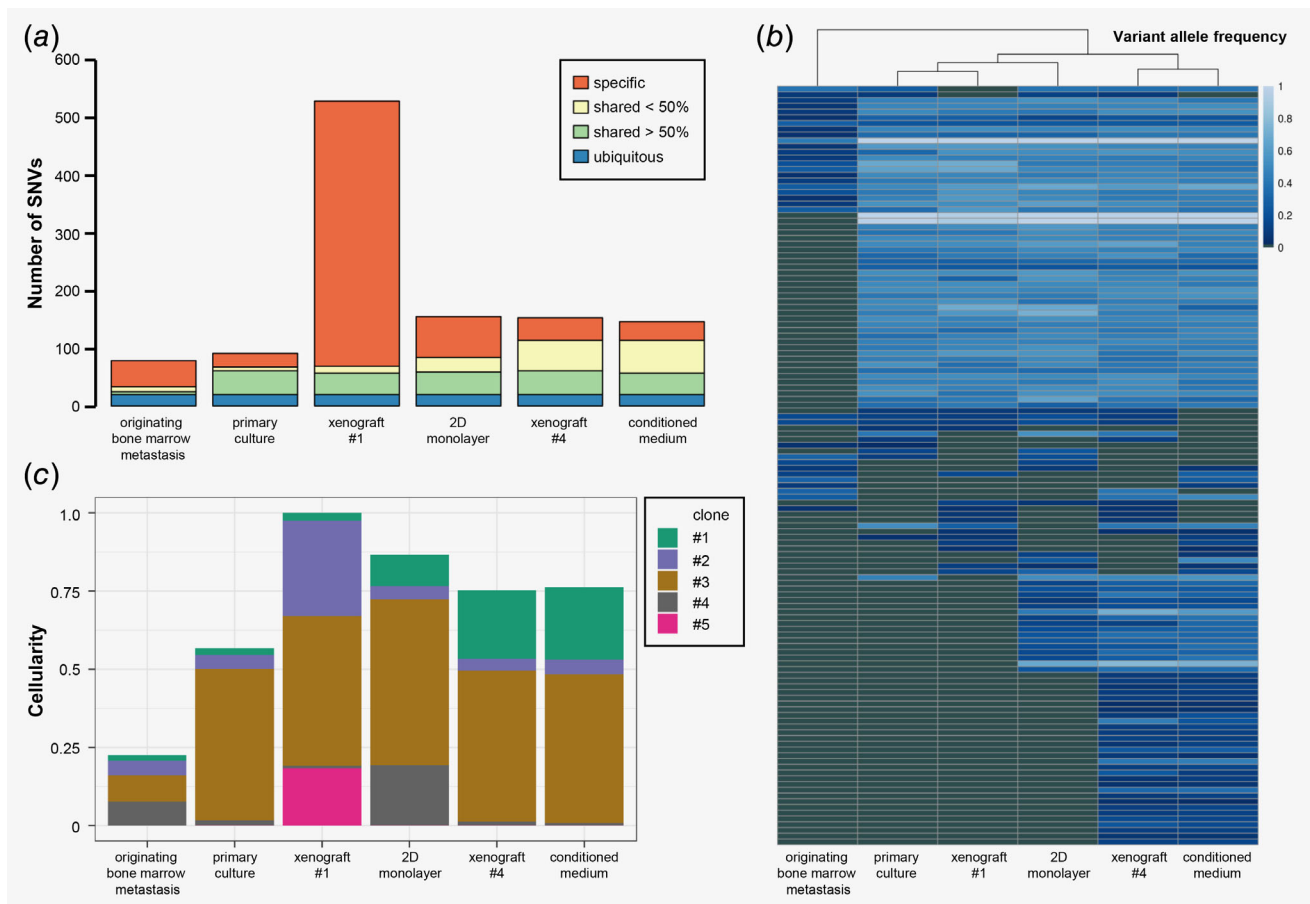


**Figure 6.** OHC-NB1 models partially reflect the heterogeneity of the originating metastasis. (a) Bar graphs of somatic SNVs in the originating bone marrow metastasis, different OHC-NB1 models or stages of OHC-NB1 model development. SNVs are categorized as occurring only in the sample indicated (specific), occurring in all samples (ubiquitous) or occurring in >50% or <50% of samples. (b) Heatmap of somatic SNVs shared by at least two samples. Frequency of SNV detection in each sample is indicated with the blue color gradient. (c) Clonal reconstruction of sample of origin and models. Each sample is displayed as a stacked column, with individual contributing clone proportions displayed by the different stacked colors in the column (stack height indicates the percentage of each clone in the model). Xenograft #1, OHC-NB1 xenograft model passage 1; xenograft #4, OHC-NB1 xenograft model passage 4; conditioned medium, medium conditioned by the intermittent *in vitro* culture of xenograft passage 4.

cancer pathogenesis and progression as well as clinical decision-making towards targeted therapeutics in mono or combination therapy approaches. Different approaches employing chromosomal aberrations and breakpoints as well as CNVs and SNVs have been developed to reconstruct the clonal composition of solid tumors.<sup>10,24</sup> Clonal reconstructions of multiregion sequencing from the same renal cell carcinoma,<sup>32</sup> high-grade glioma,<sup>33</sup> medulloblastoma<sup>34</sup> or breast cancer<sup>35</sup> revealed high-level spatial heterogeneity with individual samples having different dominant clones. Here, we demonstrate the preservation of clonal heterogeneity in the flexible patient-near OHC-NB1 neuroblastoma model system.

As intratumor genetic heterogeneity and clonal evolution have established as the normal situation in high-risk disease rather than the exception, the need for preclinical models recapitulating these traits has become more apparent. Published sequencing data of matching pairs of models and the

originating tissue are rare. In glioblastoma, a study of 10 matched pairs of cell lines and their source tumors reported an average overlap of 41% of somatic SNVs.<sup>36</sup> A comparison of *ALK* mutations in 2 cell lines and their originating neuroblastoma samples revealed that the oncogenic F1174L mutation was ubiquitous in all cells of both cell lines, but was detected in only 0.03% and 6.6% of cells in the originating tissues, indicating the *ALK* mutation provided selection pressure for the subclone in monolayer culture.<sup>14</sup> Another study applied whole-genome sequencing and array-based comparative genomic hybridization to compare eight neuroblastoma cell lines with the six primary tumors and two bone marrow metastases from which they were derived.<sup>37</sup> While *MYCN* amplification, 17q gain and 1p36 deletion were stably propagated in the cell lines, shorter CNAs differed between the cell lines and their origins, and were interpreted as potential subclonal events that were below the detection limit in the primary tumor.<sup>37</sup> The

OHC-NB1 model system presented here belongs to the first model systems capturing intratumor heterogeneity and clonal evolution for high-risk neuroblastoma. WES of the originating bone marrow metastasis and different OHC-NB1 models revealed clonal heterogeneity in the originating metastasis, recapitulation of this clonal heterogeneity in the model systems and further clonal evolution during model propagation. While most clones are shared between the originating bone marrow metastasis and models, the models differ considerably with respect to which clone(s) became dominant. These clones are also marked by nonsilent mutations in known cancer-relevant genes, which may act as secondary tumor driver events. Together, the different OHC-NB1 models reflect a heterogeneous tumor disease, in which cell clones have variable growth rates and, potentially, varying responses to therapy. The OHC-NB1 model only represents 43% of somatic SNVs and 23% of the cellularity in the source metastasis, indicating that only a subset of the neuroblastoma cells that metastasized to the bone marrow niche could be successfully propagated under the selected experimental conditions. This observation underlines the importance of further optimizing experimental workflows to fully capture the complexity of high-risk neuroblastoma in experimental models. Orthotopically xenografting patient samples may present an interesting alternative approach. Recently, orthotopically implanted patient-derived neuroblastoma and medulloblastoma xenografts were reported to maintain genetic, epigenetic, transcriptional and phenotypic stability and reflect aspects of spatial intratumor heterogeneity.<sup>38,39</sup> Generating (orthotopic) neuroblastoma patient-derived xenografts in mice is very useful, but does not support high-throughput screening and continues to be inefficient, despite the use of the most recent implantation strategies, for a subset of neuroblastomas that include tumors lacking *MYCN* amplifications or *TERT* alterations. Establishing neuroblastoma organoids from fresh samples may, therefore, represent a third preclinical neuroblastoma model, situated between the *in vitro* 2D cell lines and the *in vivo* PDX models. Organoids are 3D models of primary tumor tissue obtained from fresh biopsies, which are generated by partial mechanical or enzymatic digestion before embedding the resulting small tumor pieces in an extracellular matrix, such as Matrigel.

Recently, 3D organoids were shown to be propagated in Matrigel from various cancer types, including breast,<sup>40</sup> colon,<sup>41</sup> pancreatic,<sup>42</sup> ovarian<sup>43</sup> and prostate cancers.<sup>44</sup> While success rates of organoid establishment clearly appear to vary by tumor grade and cancer type, several studies reported that tumor-derived 3D-organoids propagated in Matrigel retain the histological and genetic features of the originating tumors and recapitulate drug responses observed in matched patients.<sup>40,45</sup> A shortcoming of classical cancer organoid cultures is the lack of stroma, blood vessels and immune cells. More recently, coculture systems have incorporated cancer-associated fibroblasts into pancreatic cancer organoids and matched tumor-derived peripheral blood lymphocytes into colon and non-small cell lung cancer organoids.<sup>46,47</sup> Organoid culture systems are, however, more costly than 2D cultures, due to the need for extracellular matrix. Here, we show that establishing OHC-NB1 neuroblastoma spheroids, as defined by spherical aggregates of tumor cells that originate from a tiny clinical bone marrow sample containing metastatic neuroblastoma cells, is technically feasible.

Intratumor heterogeneity is becoming accepted as a characteristic feature of high-risk tumors. Its implications for biomarker discovery, drug target identification, drug response, treatment decisions and resistance development make models reliably capturing intratumor heterogeneity highly valuable for preclinical drug evaluation in addition to their more encompassing recapitulation of the multiple clonal and genetic aspects of the disease. The trinity of OHC-NB1 models presented here partly reflects the genetic and clonal heterogeneity of high-risk metastatic neuroblastoma to support an accurate preclinical modeling of neuroblastoma.

### Acknowledgements

The authors thank the German NB2004 Trial Center for providing the bone marrow aspirate from which the OHC-NB1 model was derived, and Kathy Astrahantseff for comments on and editing of the manuscript. This work was supported by the German Federal Ministry of Education and Research (BMBF) through e:MED SYSMED-NB (J.H.S., 01ZX1607E; A.E., 01ZX1607A; H.E.D., 01ZX1607A), ZiSSTrans (N.B., 02NUK047E) and the European ERA-Net ERACoSysMED project OPTIMIZE-NB (A.E., 031L0087B) and by the Berlin Institute of Health through TERMINATE-NB (CRG-04; J.H.S., A.K., A.E., H.E.D.).

### References

- Park JR, Bagatell R, Cohn SL, et al. Revisions to the International Neuroblastoma Response Criteria: a consensus statement from the National Cancer Institute Clinical Trials Planning Meeting. *J Clin Oncol* 2017;35:2580–7.
- Schwab M, Alitalo K, Klempnauer KH, et al. Amplified DNA with limited homology to myc cellular oncogene is shared by human neuroblastoma cell lines and a neuroblastoma tumor. *Nature* 1983;305:245–8.
- Henrich KO, Schwab M, Westermann F. 1p36 tumor suppression – a matter of dosage? *Cancer Res* 2012;72:6079–88.
- Savellyeva L, Corvi R, Schwab M. Translocation involving 1p and 17q is a recurrent genetic alteration of human neuroblastoma cells. *Am J Hum Genet* 1994;55:334–40.
- Peifer M, Hertwig F, Roels F, et al. Telomerase activation by genomic rearrangements in high-risk neuroblastoma. *Nature* 2015;526:700–4.
- Valentijn LJ, Koster J, Zwijnenburg DA, et al. TERT rearrangements are frequent in neuroblastoma and identify aggressive tumor. *Nat Genet* 2015;47:1411–4.
- Mossé JP. Anaplastic lymphoma kinase as a cancer target in pediatric malignancies. *Clin Cancer Res* 2016;22:546–52.
- Schramm A, Koster J, Assenov Y, et al. Mutational dynamics between primary and relapse neuroblastomas. *Nat Genet* 2015;47:872–7.
- Eleveld TF, Oldridge DA, Bernard V, et al. Relapsed neuroblastomas show frequent RAS-MAPK pathway mutations. *Nat Genet* 2015;47:864–71.
- Chicard M, Colmet-Daage L, Clement N, et al. Whole-exome sequencing of cell-free DNA reveals temporo-spatial heterogeneity and identifies treatment-resistant clones in neuroblastoma. *Clin Cancer Res* 2018;24:939–49.
- Abbasi MR, Rifatbegovic F, Brunner C, et al. Impact of disseminated neuroblastoma cells on

- the identification of the relapse-seeding clone. *Clin Cancer Res* 2017;23:4224–32.
12. Chicard M, Boyault S, Colmet Daage L, et al. Genomic copy number profiling using circulating free tumor DNA highlights heterogeneity in neuroblastoma. *Clin Cancer Res* 2016;22:5564–73.
  13. Bellini A, Bernard V, Leroy Q, et al. Deep sequencing reveals occurrence of subclonal ALK mutations in neuroblastoma at diagnosis. *Clin Cancer Res* 2015;21:4913–21.
  14. Schleiermacher G, Javanmardi N, Bernard V, et al. Emergence of new ALK mutations at relapse of neuroblastoma. *J Clin Oncol* 2014;32:2727–34.
  15. Lodrini M, Oehme I, Schroeder C, et al. MYCN and HDAC2 cooperate to repress miR-183 signaling in neuroblastoma. *Nucleic Acids Res* 2013;41:6018–33.
  16. Cock JP, Fields CJ, Goto N, et al. The Sanger FASTQ file format for sequences with quality scores, and the Solexa/Illumina FASTQ variants. *Nucleic Acids Res* 2010;38:1767–71.
  17. Li H. Aligning sequence reads, clone sequences and assembly contigs with BWA-MEM. Eprint arXiv, 2013, 1303.3997.
  18. Cibulskis K, Lawrence MS, Carter SL, et al. Sensitive detection of somatic point mutations in impure and heterogeneous cancer samples. *Nat Biotechnol* 2013;31:213–9.
  19. Jäger M, Wang K, Bauer S, et al. Jannovar: a java library for exome annotation. *Hum Mutat* 2014; 35:548–55.
  20. <https://github.com/eilslabs/DKFZBiasFilter>, (08.04.2018).
  21. Forbes SA, Bindal N, Bamford S, et al. COSMIC: mining complete cancer genomes in the Catalogue of Somatic Mutations in Cancer. *Nucleic Acids Res* 2010;39:D945–50.
  22. Kuilman T, Velds A, Kemper K, et al. CopywriteR: DNA copy number detection from off-target sequence data. *Genome Biol* 2015;16:49.
  23. Griffith M, Spies NC, Krysiak K, et al. CIViC is a community knowledge base for expert crowdsourcing the clinical interpretation of variants in cancer. *Nat Genet* 2017;49:170–4.
  24. Krzywinski M, Schein J, Birol I, et al. Circos: an information aesthetic for comparative genomics. *Genome Res* 2009;19:1639–45.
  25. Deveau P, Colmet Daage L, Oldridge D, et al. QuantumClone: clonal assessment of functional mutations in cancer based on a genotype-aware method for clonal reconstruction. *Bioinformatics* 2018;34:1808–16.
  26. R Development Core Team. R: a language and environment for statistical computing. Vienna, Austria: R Foundation for Statistical Computing, 2014. <http://www.R-project.org>.
  27. Ferreira-Facio CS, Milito C, Botafogo V, et al. Contribution of multiparameter flow cytometry immunophenotyping to the diagnostic screening and classification of pediatric cancer. *PLoS One* 2013;8:e55534.
  28. Künkele A, Taraseviciute A, Finn LS, et al. Pre-clinical assessment of CD171-directed CAR T-cell adoptive therapy for childhood neuroblastoma: CE7 epitope target safety and product manufacturing feasibility. *Clin Cancer Res* 2017; 23:466–77.
  29. Bomken SN, Redfern K, Wood KM, et al. Limitations in the ability of NB84 to detect metastatic neuroblastoma cells in bone marrow. *J Clin Pathol* 2006;59:927–9.
  30. Dowsett M, Nielsen TO, A'Hern R, et al. Assessment of Ki67 in breast cancer: recommendations from the International Ki67 in Breast Cancer working group. *J Natl Cancer Inst* 2011;103: 1656–64.
  31. Fabian J, Opitz D, Althoff K, et al. MYCN and HDAC5 transcriptionally repress CD9 to trigger invasion and metastasis in neuroblastoma. *Oncotarget* 2016;7:66344–59.
  32. Gerlinger M, Rowan AJ, Horswell S, et al. Intratumor heterogeneity and branched evolution revealed by multiregion sequencing. *N Engl J Med* 2012;366:883–92.
  33. Sottoriva A, Spiteri I, Piccirillo SG, et al. Intratumor heterogeneity in human glioblastoma reflects cancer evolutionary dynamics. *Proc Natl Acad Sci U S A* 2013;110:4009–14.
  34. Morrissy AS, Cavalli FMG, Remke M, et al. Spatial heterogeneity in medulloblastoma. *Nat Genet* 2017;49:780–8.
  35. Turashvili G, Brogi E. Tumor heterogeneity in breast cancer. *Front Med* 2017;4:227.
  36. Rosenberg S, Verreault M, Schmitt C, et al. Multi-omics analysis of primary glioblastoma cell lines shows recapitulation of pivotal molecular features of parental tumors. *Neuro Oncol* 2017;19:219–28.
  37. Bate-Eya LT, Ebus ME, Koster J, et al. Newly-derived neuroblastoma cell lines propagated in serum-free media recapitulate the genotype and phenotype of primary neuroblastoma tumours. *Eur J Cancer* 2014;50:628–37.
  38. Braekvelde N, von Stedingk K, Fransson S, et al. Patient-derived xenograft models reveal intratumor heterogeneity and temporal stability in neuroblastoma. *Cancer Res* 2018;78: 5969–85.
  39. Brabetz S, Leary SES, Gröbner SN, et al. A biobank of patient-derived pediatric brain tumor models. *Nat Med* 2018;24:1752–61.
  40. Sachs N, de Ligt J, Kopper O, et al. A living biobank of breast cancer organoids captures disease heterogeneity. *Cell* 2018;172:373–86. E10.
  41. Sato T, Stange DE, Ferrante M, et al. Long-term expansion of epithelial organoids from human colon, adenoma, adenocarcinoma and Barrett's epithelium. *Gastroenterology* 2011; 141:1762–72.
  42. Boj SF, Hwang CI, Baker LA, et al. Organoid models of human and mouse ductal pancreatic cancer. *Cell* 2015;160:324–38.
  43. Maru Y, Tanaka N, Hippo Y. Efficient use of patient-derived organoids as a preclinical model for gynecologic tumors. *Gynecol Oncol* 2019;154:189–98.
  44. Gao D, Vela I, Sboner A, et al. Organoid cultures derived from patients with advance prostate cancer. *Cell* 2014;159:176–87.
  45. Vlachogiannis G, Hedayat S, Vatsiou A, et al. Patient-derived organoids model treatment response of metastatic gastrointestinal cancers. *Science* 2018;359:920–6.
  46. Öhlund D, Handly-Santana A, Biffi G, et al. Distinct populations of inflammatory fibroblasts and myofibroblasts in pancreatic cancer. *J Exp Med* 2017;214:579–96.
  47. Dijkstra KK, Cattaneo CM, Weeber F, et al. Generation of tumor-reactive T cells by co-culture of peripheral blood lymphocytes and tumor organoids. *Cell* 2018;174:1586–98.